Journal of Cardiology (2010) 56, 97—110

available at www.sciencedirect.com

ScienceDirect

journal homepage: www.elsevier.com/locate/jjcc

Original article

Spiral systolic blood flow in the ascending aorta and aortic arch analyzed by echo-dynamography

Motonao Tanaka (MD, FJCC)[a,*], Tsuguya Sakamoto (MD, FJCC)[b], Shigeo Sugawara (MD, FJCC)[a], Hiroyuki Nakajima (RMS)[a], Takeyoshi Kameyama (MD)[a], Yoshiaki Katahira (MD)[a], Shigeo Ohtsuki (PhD)[c], Hiroshi Kanai (PhD)[d]

[a] *Cardiovascular Center, Tohoku Welfare Pension Hospital, Fukumuro 1-12-1, Miyagino-ku, Sendai, 983-0005, Japan*
[b] *Hanzohmon Hospital, Kojimachi 1-14, Chiyoda-ku, Tokyo 102-0083, Japan*
[c] *Institute of Medical Ultrasound Technology, Yokoyama 2-12-15, Sagamihara252-0242, Japan*
[d] *Department of Electrical Engineering, Tohoku University, Aramaki-Aoba6-6-05, Aoba-ku, Sendai 980-8579, Japan*

Received 9 February 2010; accepted 8 March 2010
Available online 13 May 2010

KEYWORDS
Flow structure;
Twisted spiral flow;
Vorticity;
Changing acceleration of the flow direction;
Velocity vector distribution;
Ascending aorta;
Echo-dynamography

Summary Using echo-dynamography, systolic blood flow structure in the ascending aorta and aortic arch was investigated in 10 healthy volunteers. The blood flow structure was analyzed based on the two-dimensional (2D) and 1D velocity vector distributions, changing acceleration of flow direction (CAFD), vorticity distribution, and Doppler pressure distribution. To justify the results obtained in humans, in vitro experiments were done using straight and curved tube models of 20 mm diameter.

The distribution of the CAFD showed a spiral staircase pattern along the flow axis line. In addition, the changes in the velocity profile in the short-axis direction, 2D distribution of the vorticity, and velocity vector distribution on the aortic cross-section plane, all confirmed the presence of systolic twisted spiral flow rotating clockwise toward the peripheral part of the ascending aorta.

The rotation cycle of this spiral flow correlated inversely with the maximum velocity of the aortic flow, so that this cycle was shorter in early systole and longer in late systole. The model experiments showed similar results.

The spiral flow seemed to be produced by several factors: (i) anterior shift of the direction of ejected blood flow due to the anterior displacement of the projection of the aorta; (ii) accelerated high pressure flow ejected antero-upward; (iii) inertia resistance at the peripheral boundary of the sinus of Valsalva; and (iv) reflection caused by the concave spherical structure of the inner surface of the basal part of the aorta.

* Corresponding author. Tel.: +81 22 719 5161; fax: +81 22 719 5166.
E-mail address: m.tanaka@jata-miyagi.org (M. Tanaka).

0914-5087/$ — see front matter
doi:10.1016/j.jjcc.2010.03.008

Because the main spiral flow axis line nearly coincided with the center line of the aorta, it is concluded that the occurrence of the spiral flow plays an important role in maintaining the blood flow direction passing through the cylindrical curved aortic arch and thus in keeping the most effective ejection as well as in dispersing the shear stress in the aortic wall.

Introduction

The structure of the accelerated blood flow accompanying high pressure in the ascending aorta during the very short ejection period seems to be complicated because of the specific truncal anatomy of the aorta and the cylindrical curved structure of the inner surface of the aortic arch.

Accordingly, the blood flow structure and the flow dynamics have been of interest in both clinical [1,2] and experimental [3—5] fields including computer simulation [6,7]. However, the flow structure in the aorta in a human being [8] has not been definitely clarified because of the lack of a suitable technique for measuring the flow structure.

Recently, magnetic resonance imaging (MRI) [9] and the color Doppler method [10] have been proposed to measure the aortic flow. The former disclosed the helical flow [9], but the spatial resolution (ca 8—10 mm) is not enough for accurate measurement. The ultrasonic method has difficulty in obtaining the velocity as the vector.

In the present study, echo-dynamography [9—12] was utilized to investigate the flow structure in the ascending aorta and aortic arch and to disclose the specific characteristics.

Subjects and methods

Subjects

Ten presumably healthy adult volunteers aged from 20 to 50 years were the subjects of this study.

Methods

Analysis of the human blood flow structure in the left ventricle and aorta: in vivo study

Acquisition of the flow velocity data by ultrasound. Commercially available ultrasonic equipment (model 6500, Aloka Co., Tokyo, Japan) was used. The ultrasonic frequency was 3 MHz, and supine or left lateral decubitus position was selected. Two-dimensional (2D) echocardiograms were recorded whenever 2D sector scan with transthoracic apical or parasternal approach was required. The most advantageous long axis was selected to analyze blood flow in the ventricle, and the longitudinal section to the ascending aorta including the anterior part of the aortic arch was also selected.

After the 2D Doppler velocity data were recorded, all the data were transferred to a personal computer through magneto-optical disk memory. The Doppler flow velocity data were processed off-line by using software for echo-dynamography [11].

Detection of blood flow velocity vector and its representation. The orthogonal velocity component to the ultrasonic beam direction was deduced from the Doppler velocity data by using the flow function theory [11,13] of fluid mechanics [14]. Then, the 2D distribution of flow velocity vector in various points was calculated from the 2 velocity components, the one that was in the beam direction and the other, in the orthogonal direction.

The magnitude of the velocity vector was shown by the length of a yellow line and the standard length of the vector as a reference (20 cm/s etc.) at the left upper corner of the screen. The direction of the vector was indicated by the inclination of a yellow line with a red mark at the tip.

The blood flow velocity vector overlapped with 2D echocardiogram was depicted by the following 5 display manners.

(i) 2D distribution of the vector overlapped with 2D echocardiogram (Fig. 1, left),
(ii) 1D distribution of the vector overlapped with 2D echocardiogram to display (a) and (b); i.e.
  (a) velocity vector on the central axis line of the aorta displayed perpendicularly to the center line of the aorta (Fig. 2, right),
  (b) the vector on the central axis line along this line (Fig. 2, left).
(iii) 2D distribution of the velocity vector on the short-axis cross-section plane (Fig. 1, right)
(iv) velocity profile in the short-axis direction of the aorta (Fig. 3)

Measurement of the vorticity and its representation. To observe the various eddy components involved in the ejected blood flow, the vorticity (ω) [14] was calculated from the rotation of the flow velocity vector in many places on the scanning plane and overlapped with 2D echocardiogram by color (Fig. 6, left). The positive vorticity was shown by warm color and the negative one by cold color.

Measurement of the 2D distribution of the changing acceleration of flow direction. The information regarding the effect of the shape and structure of the aortic pathway to instantaneously changing blood flow direction was obtained quantitatively to estimate the flow structure and flow dynamics. The product of the vorticity (ω) and the velocity vector (v), which is defined as ''changing acceleration of flow direction (CAFD) ($v \cdot \omega$)'' was calculated [15].

From the 2D distribution of this acceleration and the 1D distribution in the central line of the aorta, characteristics of the flow structure in the aorta were analyzed. The magnitude of the acceleration vector was indicated by the length of a blue line, and the direction was shown by the inclination of the vector having a red mark at the tip.

Measurement of the Doppler pressure distribution. To deduce the dynamic pressure from the distribution of the flow velocity data, the Navier—Stokes' equation of motion was applied for processing the Doppler velocity data, and

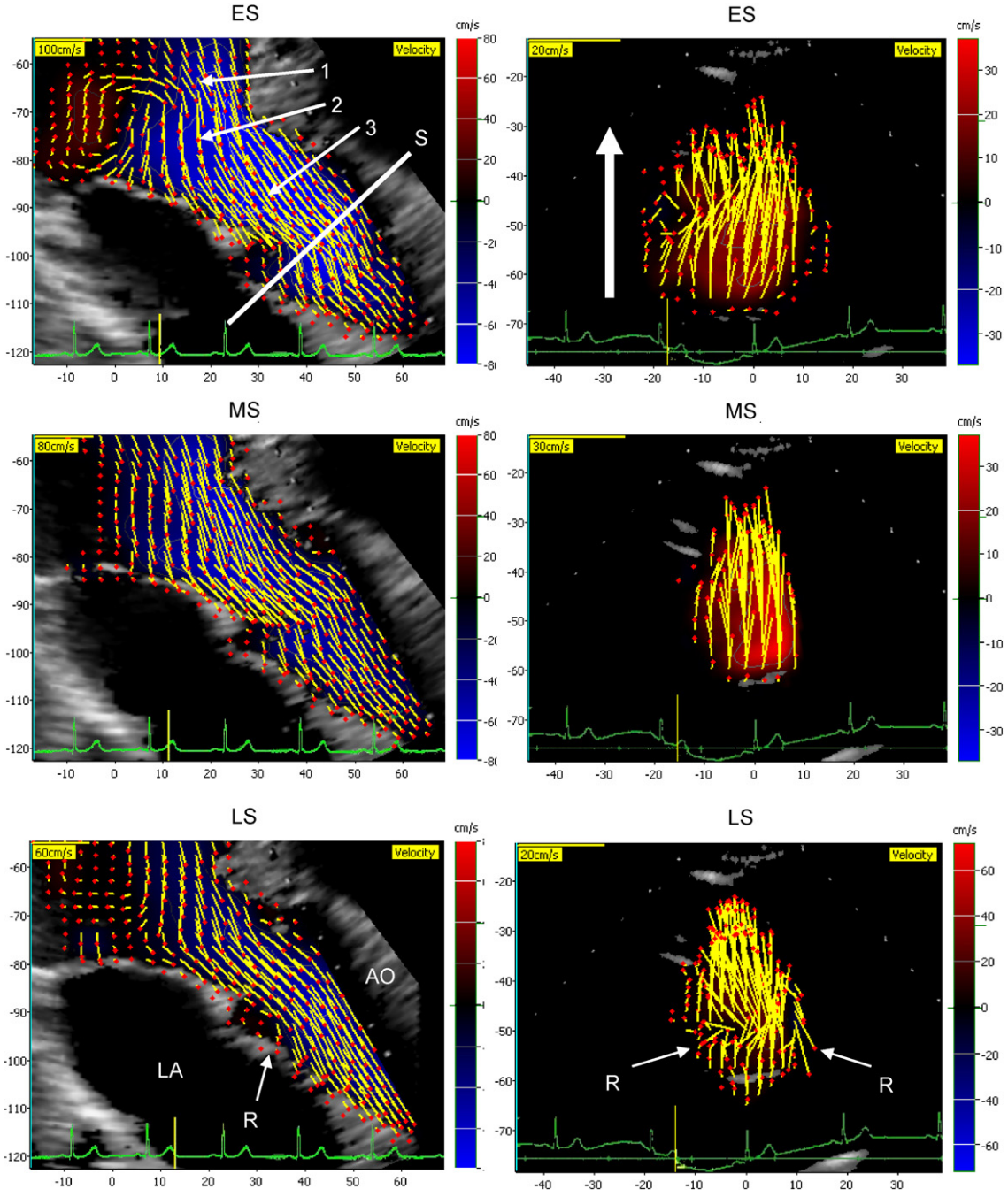

Figure 1 *Left*: Two-dimensional (2D) mapping of flow velocity vector on the longitudinal section plane of the ascending aorta during systole in a healthy adult. The timing is shown on the ECG by a yellow line and the magnitude of the vector is indicated by the length of the yellow line. The direction is displayed by the inclination of yellow lines with a red mark at the tip. Reference of the vector is shown by the yellow bar at the left upper corner of the figure. AO, aorta; LA, left atrium; ES, early systolic phase; MS, mid-systolic phase; LS, late systolic phase. *Right*: 2D mapping of the velocity vector on the cross-section of the ascending aorta. The section plane set in the short-axis direction corresponding to the white line (S) shown in Fig. 1 ES. Clockwise rotation of the vector observed. Thick arrow (ES, right) indicates the flow direction. R, reversal flow appeared in late systole. (For interpretation of the references to color in this figure legend, the reader is referred to the web version of the article.)

the theory of Helmholtz was applied to transfer from the velocity information as a vector value to the pressure information as a scalar value [16,17]. The latter was demonstrated by color overlapped with 2D echocardiogram. Positive component of the pressure was displayed with warm color and negative one by cold color.

Detailed pressure distribution was estimated by the 1D display of a red line graph (Fig. 6, right).

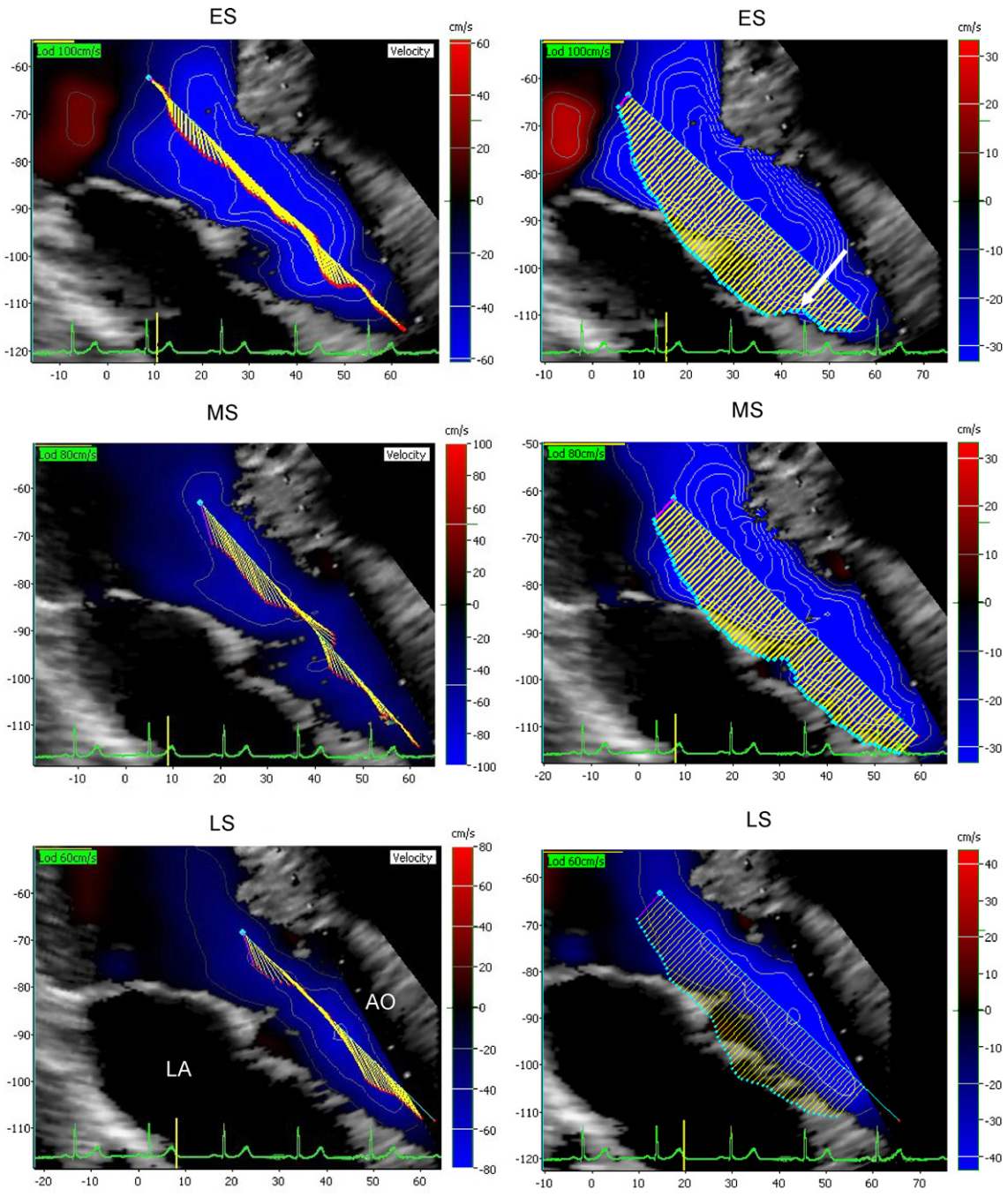

Figure 2 *Left*: One-dimensional (1D) display of the flow velocity vector along the longitudinal axis line of the ascending aorta. Twisted pattern of the velocity vector is demonstrated along the axis line. *Right*: 1D distribution of the magnitude of the velocity vector along the flow direction on the longitudinal axis line of the ascending aorta. The magnitude of the vector is shown perpendicular to this axis by the yellow bar. The maximum velocity abruptly decreases to about 50% due to the inertia resistance at the distal margin of the sinus of Valsalva in ES (white arrow). AO, aorta; LA, left atrium; ES, early systolic phase; MS, mid-systolic phase; LS, late systolic phase. (For interpretation of the references to color in this figure legend, the reader is referred to the web version of the article.)

''In vitro'' experiment

As the flow model, an optically and acoustically transparent vinyl tube of 20 mm internal diameter and 2 mm in thickness was used. The models were 2 types, one, a straight tube of 1 m in length, the other, a curved tube with 70 mm in its radius of curvature (Fig. 9). These tubes were set in such conditions that the central axis line of the tube was horizontal to avoid a pressure difference between the inlet and outlet of the tube, and were fixed by immersing in ca 3% transparent agar solution.

For optical and acoustic observations of the flow structure, a minute particle of ion exchange resin (Amberlite,

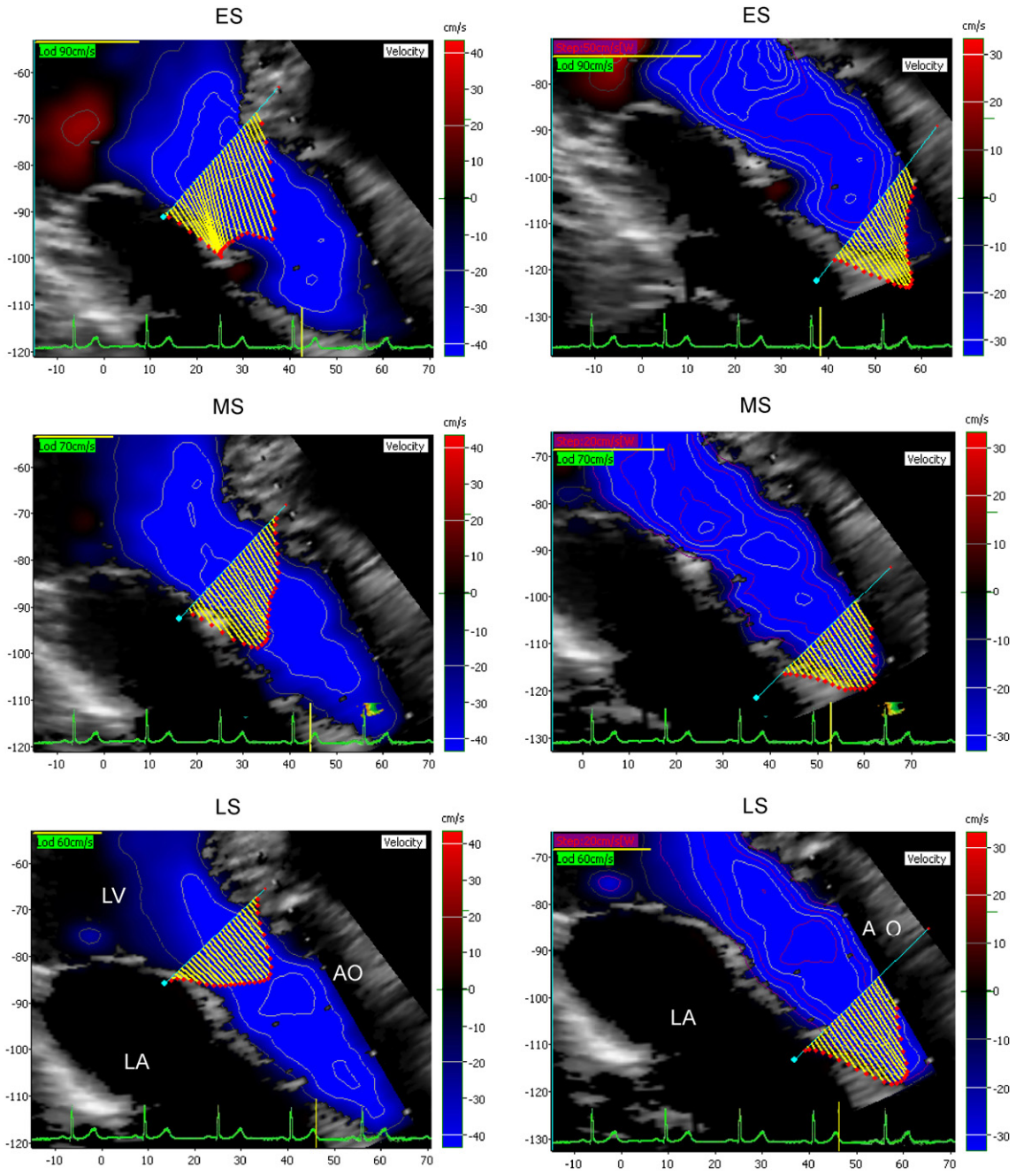

Figure 3 *Left*: Flow velocity profiles in the short-axis direction at the subvalvular outflow tract area. *Right*: Flow velocity profiles at the area near the peripheral edge of the sinus of Valsalva. Reference of the vector shows at the left upper corner of the figure. LA, left atrium; LV, left ventricle; AO, aorta; ES, early systolic phase; MS, mid-systolic phase; LS, late systolic phase.

Rohm and Haas, Philadelphia, PA, USA) of about 10—15 μm mixed in 20—30% glycerine solution were used, the density of which was adjusted to the viscosity of blood. The speed of the flow was about 1—1.5 m/s, which was nearly identical to the velocity of blood flow in a normal subject.

To measure the flow velocity by the ultrasonic Doppler method, the sector scanning plane was horizontal to the longitudinal section plane which includes the central flow axis line of the model. The flow velocity was obtained by the color Doppler method. At the same time, flat light of 2 mm in thickness was shed to the flow horizontally as in the case of the ultrasonic scanning plane, and high frame rate photographs were recorded perpendicularly to the flat light plane, so as to analyze the flow structure optically.

Results

In vivo study

2D distribution of the blood flow velocity vector in the ascending aorta

Initially, the direction of the blood flow velocity vector in early systole (ES) was antero-upward in the outflow tract area (1 in Fig. 1), whereas it was postero-downward in the

basal area of the aorta (2 in Fig. 1), and then antero-upward again in the ascending aorta (3 in Fig. 1), resulting in a zigzag pattern. About 100 ms later (in mid-systole, MS), this zigzag pattern was nearly constant while it gradually subsided in late systole (LS).

2D distribution of the velocity vector on the oblique cross-section plane (ca 45°) of the ascending aorta (white line S in Fig. 1, left) disclosed that the direction of this vector inclined right obliquely in the area near the anterior wall and further left near the posterior wall (Fig. 1, right).

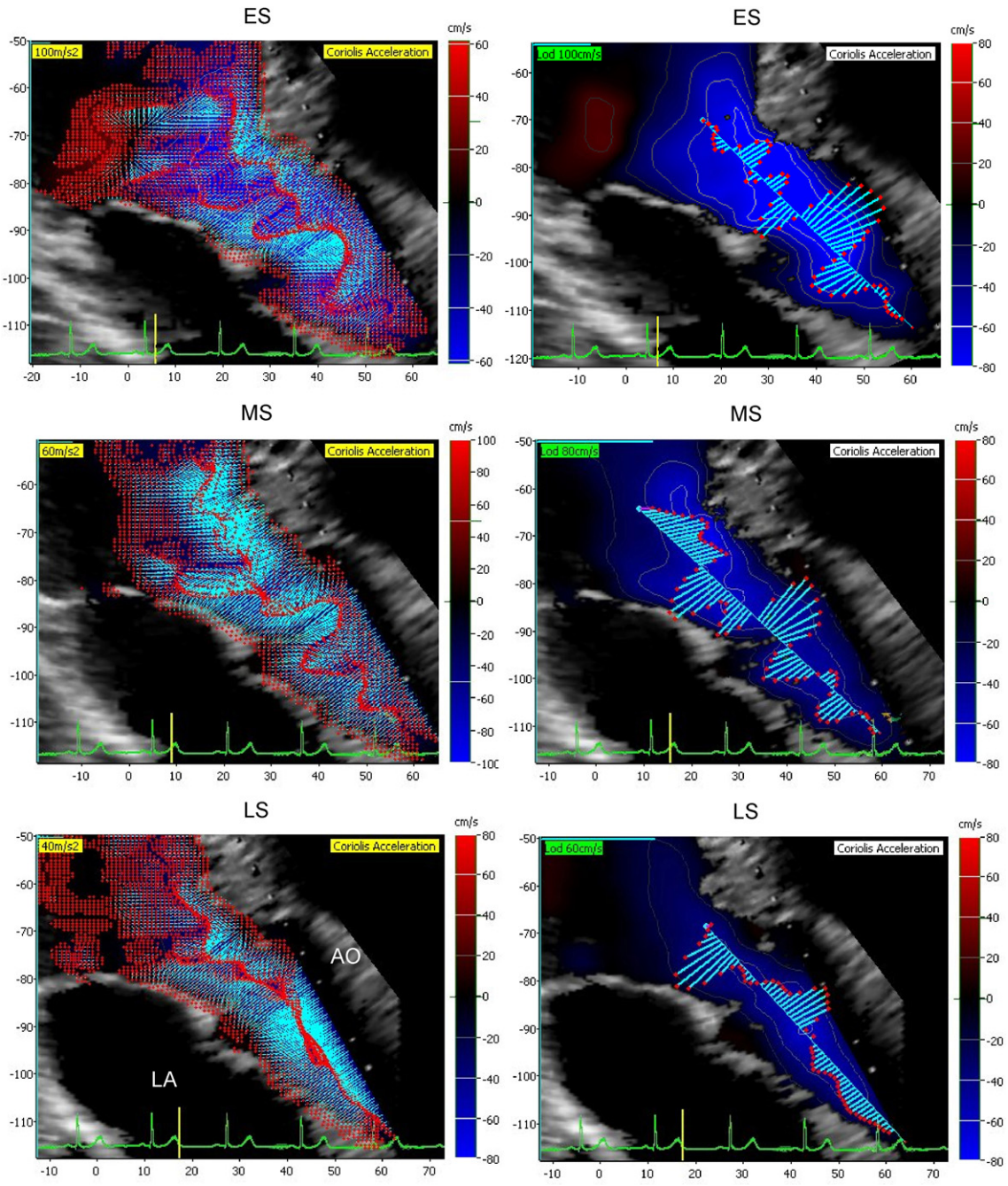

Figure 4 1D (right) and 2D (left) distribution of the changing acceleration of flow direction (CAFD) in the ascending aorta. The magnitude of the acceleration vector is indicated by the length of blue line and the direction of the vector is shown by the inclination of the blue bar with the red tip. In the 2D distribution, semi-circular radial distribution of the vector originated from the aortic inner wall is arranged alternately in the anterior or posterior wall of the aorta. The tip of the vector is figured as a wave pattern in ES and MS, and as a linear pattern in LS (left). In the 1D distribution, the acceleration vector appeared perpendicularly from the center line of the aorta, and shows a radial pattern, which is demonstrated alternately in the anterior or posterior direction from the center line. Assuming the 3D flow, the CAFD distribution looks like a spiral staircase. LA, left atrium; AO, aorta; ES, early systolic phase; MS, mid-systolic phase; LS, late systolic phase. (For interpretation of the references to color in this figure legend, the reader is referred to the web version of the article.)

This confirmed the presence of the clockwise rotation of blood flow in the ascending aorta. In LS, reversal blood flow vectors separating from the main flow were observed at the basal part near the aortic wall (R in Fig. 1, LS).

The flow velocity vector profile on the long-axis line of the aorta

The tip of the flow velocity vector along the center line of the ascending aorta alternatively shifted anteriorly or posteriorly. This means that the vector was twisted (Fig. 2, left).

As seen in the 1D distribution of the velocity vector profile along the longitudinal-axis line of the ascending aorta, the flow velocity was maximum at the basal part and decreased abruptly about 50% at the distal margin in the sinus of Valsalva in the ES (Fig. 2, right, white arrow). In MS and afterward, velocity gradient in the basal part gradually decreased and was steady in LS (Fig. 2, right). This abrupt decrement of the velocity indicated the presence of the inertia resistance from the blood in the peripheral aortic route.

The flow velocity vector profile on the short-axis line of the aorta

In the short-axis direction, analysis of the velocity profile in the plane of aortic curvature beneath the aortic valve disclosed a large flow velocity vector in the outer layer in ES, whereas it was small in the inner layer, so that a velocity gradient developed between these 2 layers (Fig. 3, left, ES). The inclination of the velocity gradient curve was smooth and the fast component was about twofold compared with the slow one. In MS (nearly 100 ms later), this gradient was reversed, and in LS (further delay of ca 100 ms), the velocity profile again showed the reverse, giving a sharp triangle pattern with the largest velocity vector at the central part of the aorta. On the other hand, at the area near the boundary of the distal margin of the sinus of Valsalva (about 20 mm distant from the aortic orifice), the largest vector appeared in the inner layer, whereas it was small in the outer layer of the aortic arch (Fig. 3, right). In MS, (about 100 ms later), the largest vector appeared at the central part, and the location in the LS was at the center part of the aorta. In the

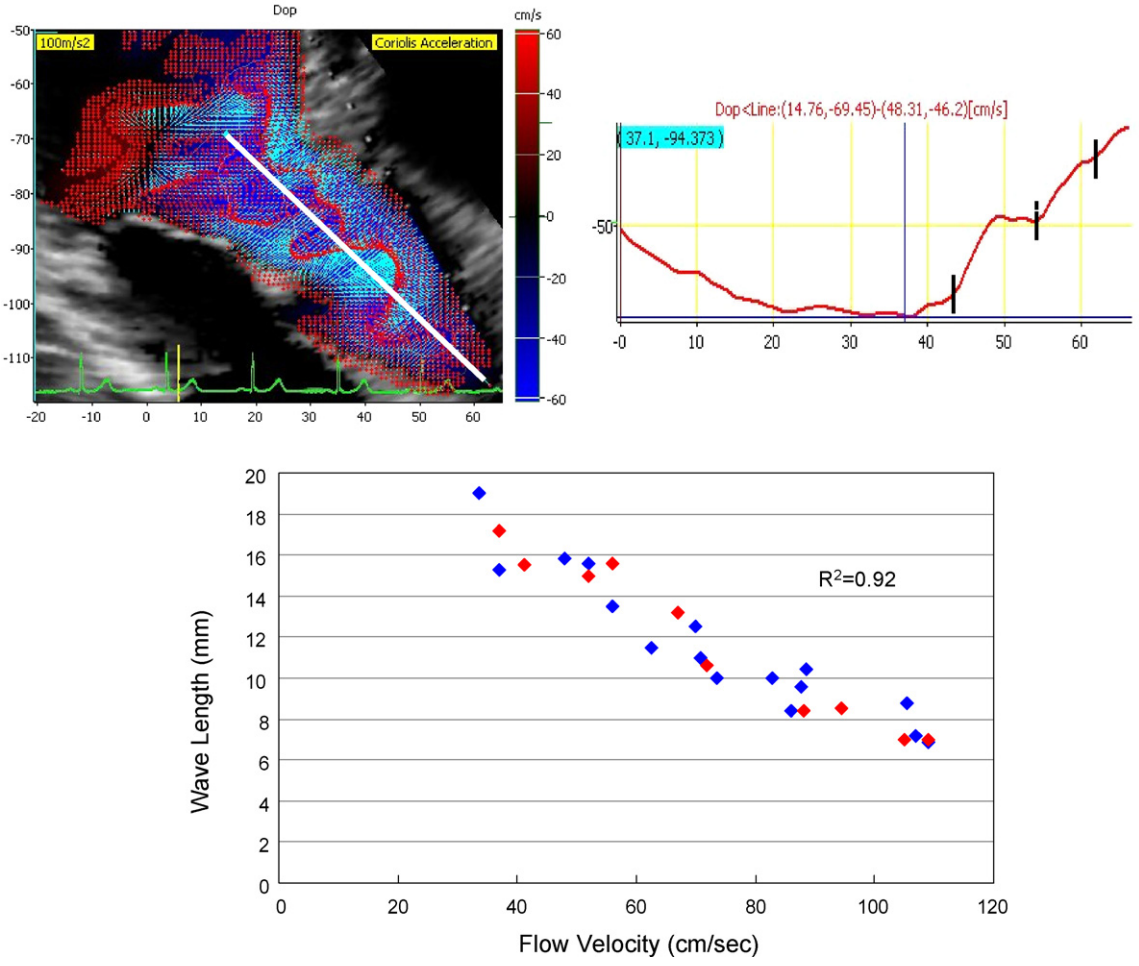

Figure 5 Upper two figures are 2D and 1D distribution of the changing acceleration of flow direction (CAFD) in early systole. Right graph shows the acceleration vector distribution along the white line in the left figure, and an interval between two black bars on the graph indicates the wave length of the wave pattern of the 2D distribution of the CAFD. Lower figure shows the correlation between the wave length and the maximum flow velocity in the pathway in vitro (blue) and in vivo (red). Negative correlation is presented. (For interpretation of the references to color in this figure legend, the reader is referred to the web version of the article.)

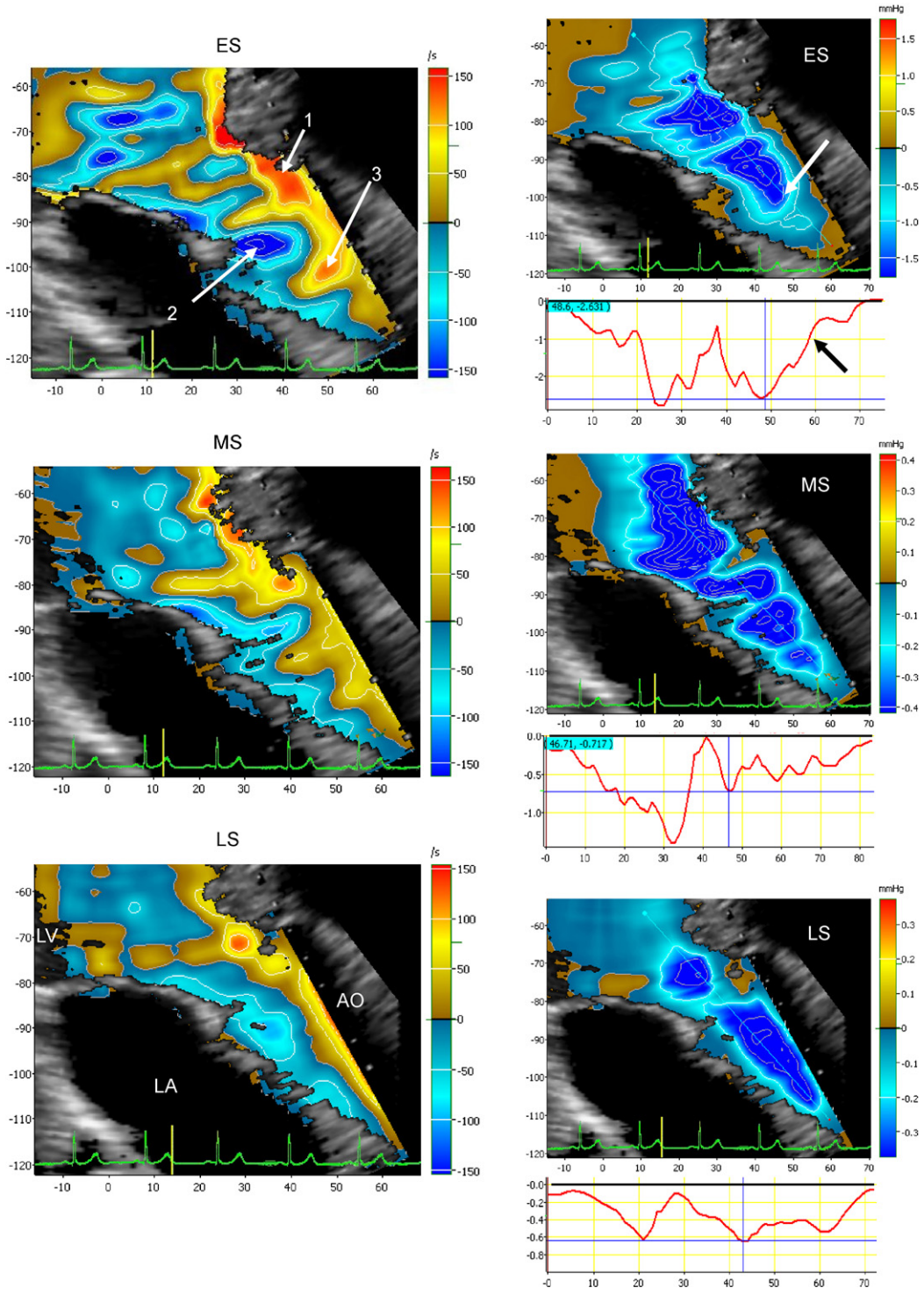

Figure 6 *Left*: 2D distribution of the vorticity in the left ventricle and aorta in ejection phase. Positive vorticity is shown by the warm color and negative vorticity, cold one. The grade of the vorticity is estimated by the color bar in the right side of the figure. The positive vorticity appears in the area near the antero-upper wall and the negative one, near the postero-lower wall of the ascending aorta. The maximum vorticity appears alternately. This finding indicates that strong rotation occurs in the basal part of the aorta. (1) Initial rotation, (2) 2nd rotation, and (3) 3rd rotation. *Right*: 2D distribution of the Doppler pressure in the left ventricle and aorta. Cold color area means a negative pressure and warm color area, a positive one. Reference point is set at the aortic valve ring. The negative pressure (about −3 mm Hg) areas appear in both the outflow tract area beneath the aortic valve and the basal part of the ascending aorta in ES. Rapid pressure increase due to the inertia resistance occurs at the distal margin of the sinus of Valsalva (black and white arrows in ES). Thereafter, the pressure gradient becomes small with the time course (MS, LS). The minimum Doppler pressure area appears along the center line of the ascending aorta and arch. LA, left atrium; LV, left ventricle; AO, aorta; ES, early systolic phase; MS, mid-systolic phase; LS, late systolic phase.

space between the basal area of the outflow tract beneath the aortic orifice and the distal margin of the sinus of Valsalva, the reversed velocity gradient was observed at every certain time interval from the onset of the ejection and at every certain distance from the orifice. The equilateral triangular or sharpened parabolic velocity profile (Fig. 3, LS) seemed to be produced by the rolling friction in the rotating flow.

These results indicate that the strong rotation occurred in this space, and the maximum velocity vector in the ascending aorta appeared at the central part during systolic phase, resulting in the rotation flow in the ascending aorta.

2D distribution of the CAFD in the ascending aorta

A more detailed figure of the second parameter of this rotation was evaluated by CAFD. In the ES and MS, 2D distri-

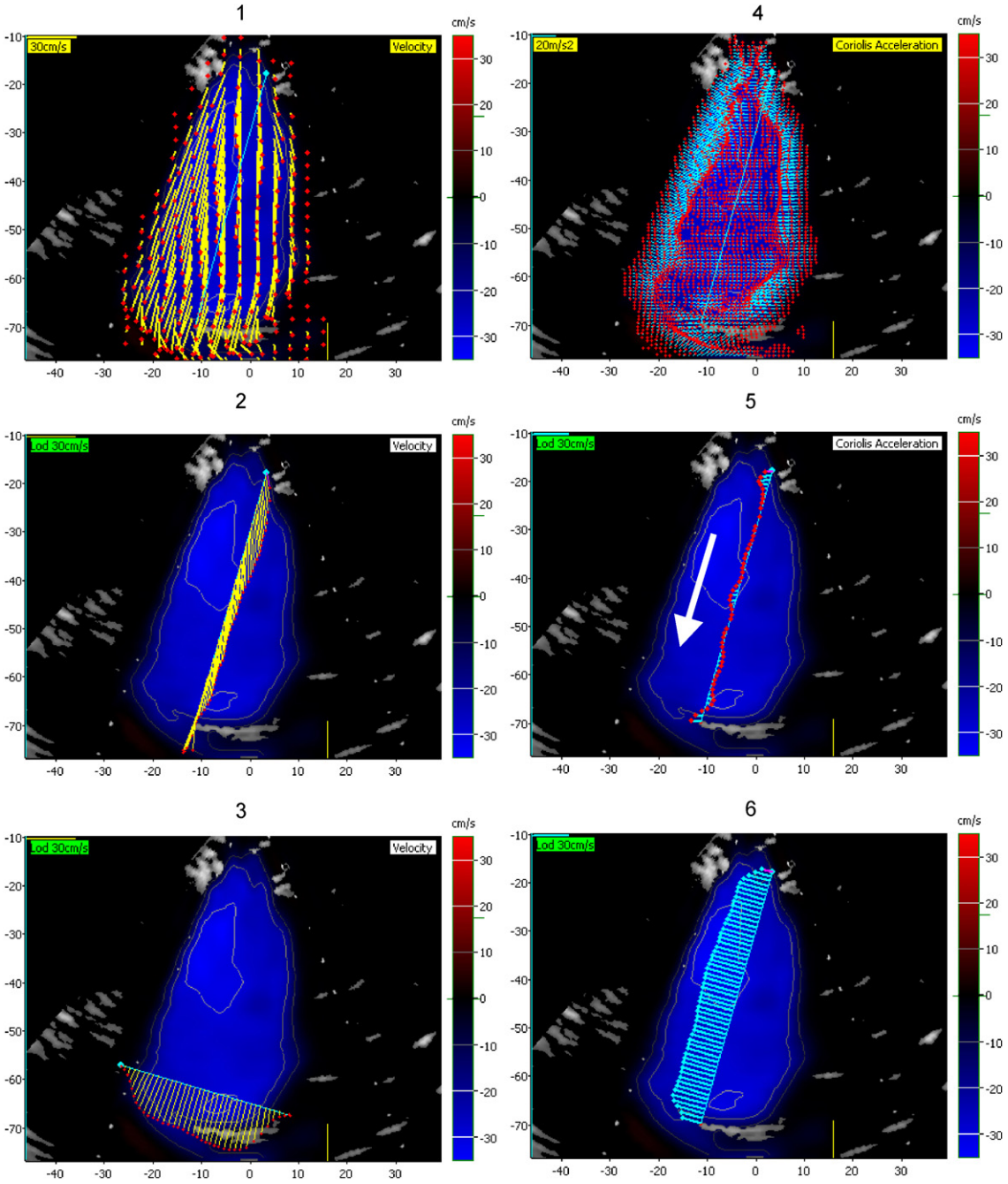

Figure 7 Experimental results obtained by using the straight tube model. 1, 2D distribution of the flow velocity vector; 2, 1D distribution of the flow velocity vector on the center line of the tube along the flow axis; 3, Flow velocity profile in the short-axis direction; 4, 2D distribution of the CAFD; 5, 1D distribution of the CAFD on the center line of the tube along the flow direction; 6, Flow velocity profile in the long-axis direction. White arrow indicates the flow direction. CAFD, changing acceleration of flow direction.

bution of CAFD on the longitudinal section plane of the aorta demonstrated a fan of the radial pattern from the inner surface of the aortic wall (Fig. 4, left). Many radially arranged vectors alternately appeared from the anterior or posterior wall of the aorta. Thus, the line connecting the tips of the acceleration vector constituted a red snaky pattern in the central area of the aorta. As systole progressed (LS), the acceleration vector originated perpendicularly from the wall into the blood, therefore, the line connected with the tips of the vector tended toward the linear pattern.

CAFD along the central-axis line of the aorta showed a pattern of the radial vector distribution alternately toward the opposite direction. The line connecting with the tips of the vector showed a wave pattern. Thus, it was disclosed that, three-dimensionally, the spiral staircase acceleration vector developed in the ascending aorta.

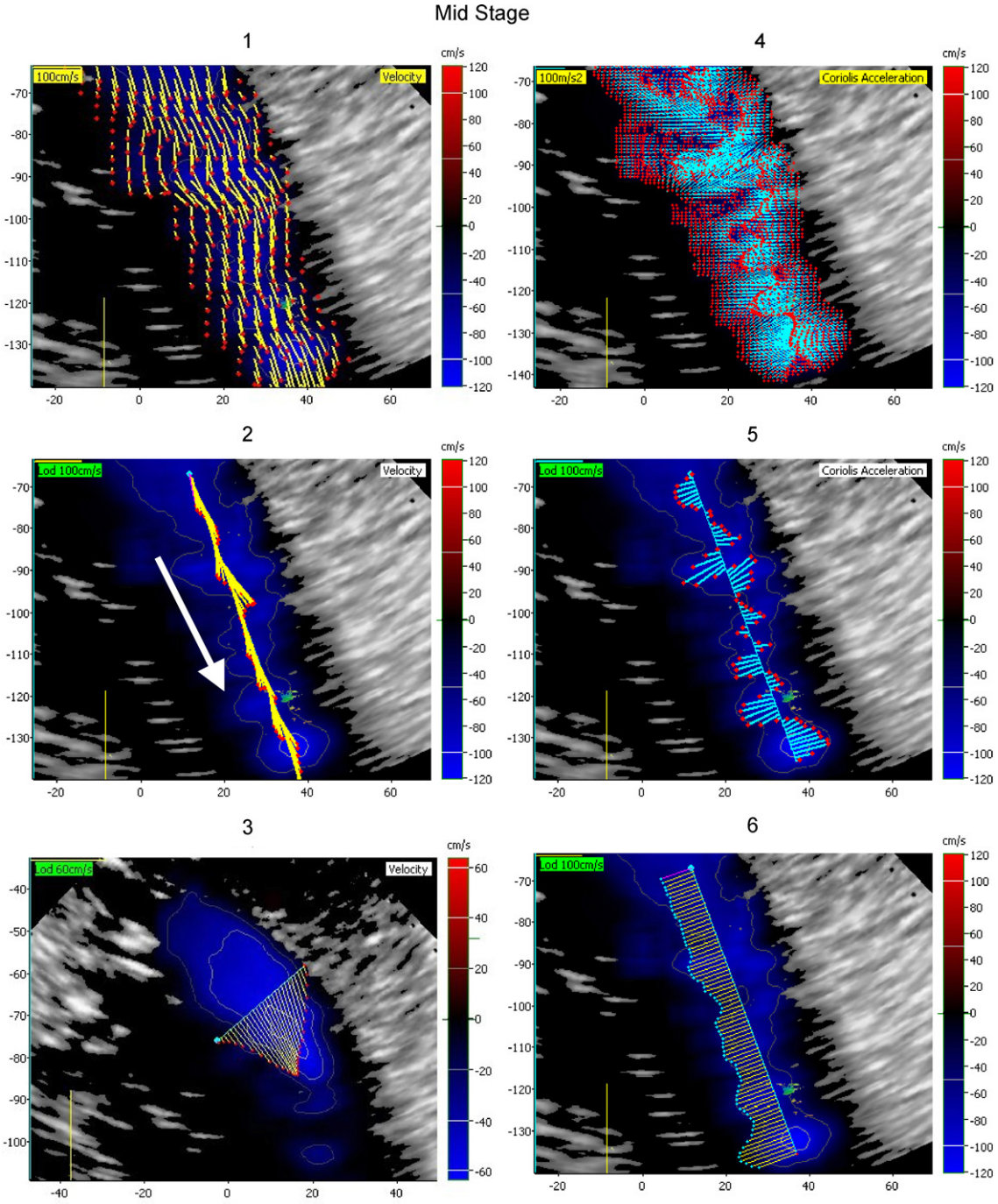

Figure 8 Results experimentally obtained by using the curved tube model. 1, 2D distribution of the flow velocity vector; 2, 1D distribution of the flow velocity vector on the center line of the tube along the flow axis; 3, Flow velocity profile in the short-axis direction; 4, 2D distribution of the CAFD; 5, 1D distribution of the CAFD on the center line of the tube along the flow direction; 6, Flow velocity profile in the long-axis direction of the tube model. White arrow indicates the flow direction. CAFD, changing acceleration of flow direction.

The magnitude of the CAFD in ES was large in the anterosuperior direction at the basal part of the ascending aorta compared to that in the peripheral part. On the other hand, the magnitude in the peripheral part became larger in MS and LS, indicating the occurrence of large rotation of the blood flow in the basal part of the aorta and progression to the peripheral part of the aorta with time course.

The wave length of the wave pattern figured by the tip of the acceleration vector had an inverse correlation with the maximum velocity in the aorta (Fig. 5), i.e. the higher the velocity, the faster the rotation.

2D distribution of the vorticity of the blood flow in the ascending aorta

One parameter of this rotation was the vorticity of the ejecting flow. At the beginning of the ejection (Fig. 6, left), the maximum area of the positive vorticity (red area, 100—150/s) appeared at the anterior part of the outflow tract beneath the aortic valve. On the other hand, the negative vorticity area (blue area, −100 to −150/s) appeared posteriorly just above the aortic valve (2nd rotation (2)). These positive (+) and negative (−) components of the vorticity alternately appeared toward the peripheral part and the vorticity gradually decreased after MS, both indicating the strong rotation produced at the part from the outflow tract to the basal part of the aorta.

2D distribution of the Doppler pressure in the ascending aorta

About −3 mm Hg negative pressure was shown in both the outflow tract area beneath the valve ring and the basal area of the aorta in the ES (Fig. 6, right). An abrupt pressure increase occurred at the peripheral margin of the sinus of Valsalva (Fig. 6, right, white and black arrows). Following MS, the pressure difference was restored and reached the level of 0.5—0.8 mm Hg, thus the pressure curve also showed a cyclic pattern.

In vitro study

Straight tube flow model

2D distribution of the flow velocity vector in the straight tube model showed a parallel pattern (Fig. 7-1). 1D distribution of the velocity vector on the center line along the flow direction (Fig. 7-2) and the velocity profile in the short-axis direction showed a lineal flow character parallel to the tube wall (Fig. 7-3 and -6).

2D distribution of the CAFD showed a laminar pattern with nearly the same magnitude of acceleration vector perpendicularly to the tube wall (Fig. 7-4). The rectangular component of the acceleration described in the curved tube was not observed in 1D distribution of the CAFD (Fig. 7-5).

Curved tube flow model

As shown in Fig. 8, all of the information regarding the flow structure such as 2D and 1D distribution of the flow velocity vector along the longitudinal direction, flow velocity profile in the short-axis direction, 2D and 1D distribution of the CAFD along the main flow axis line, and the correlation between flow velocity and wave length of the wave pattern in 2D distribution, all showed nearly the same results as those obtained in the clinical observation. Clockwise rota-

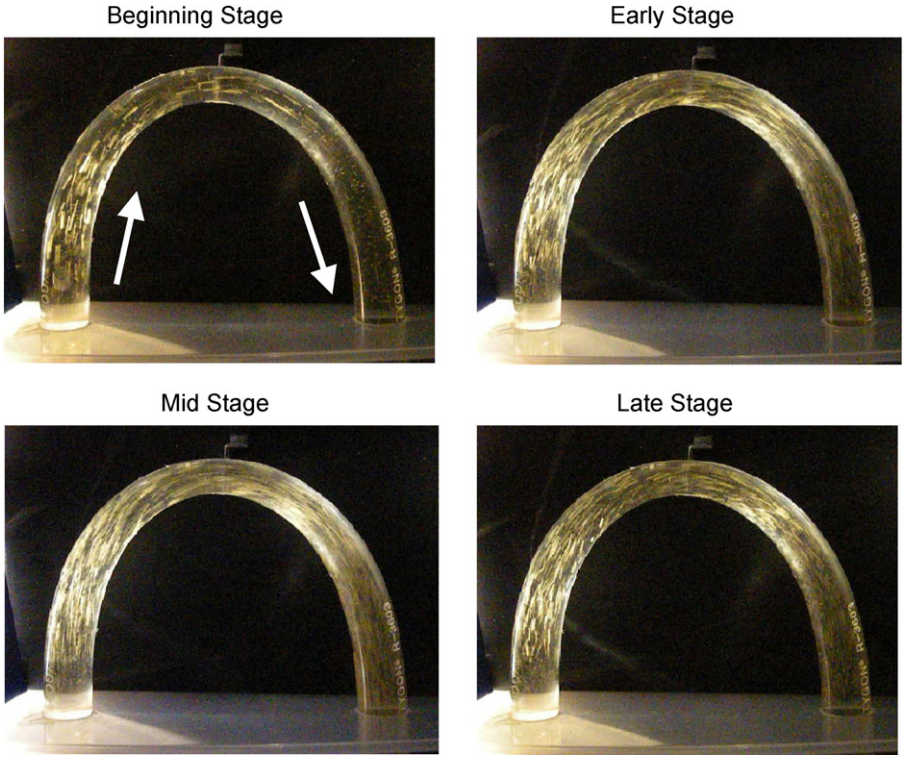

Figure 9 Flow visualization in the curved model at the 4 stages in pulsatile flow. The effects of the curvature of the tube are shown and the centralized rotating flow is also observed. White arrow indicates the flow direction.

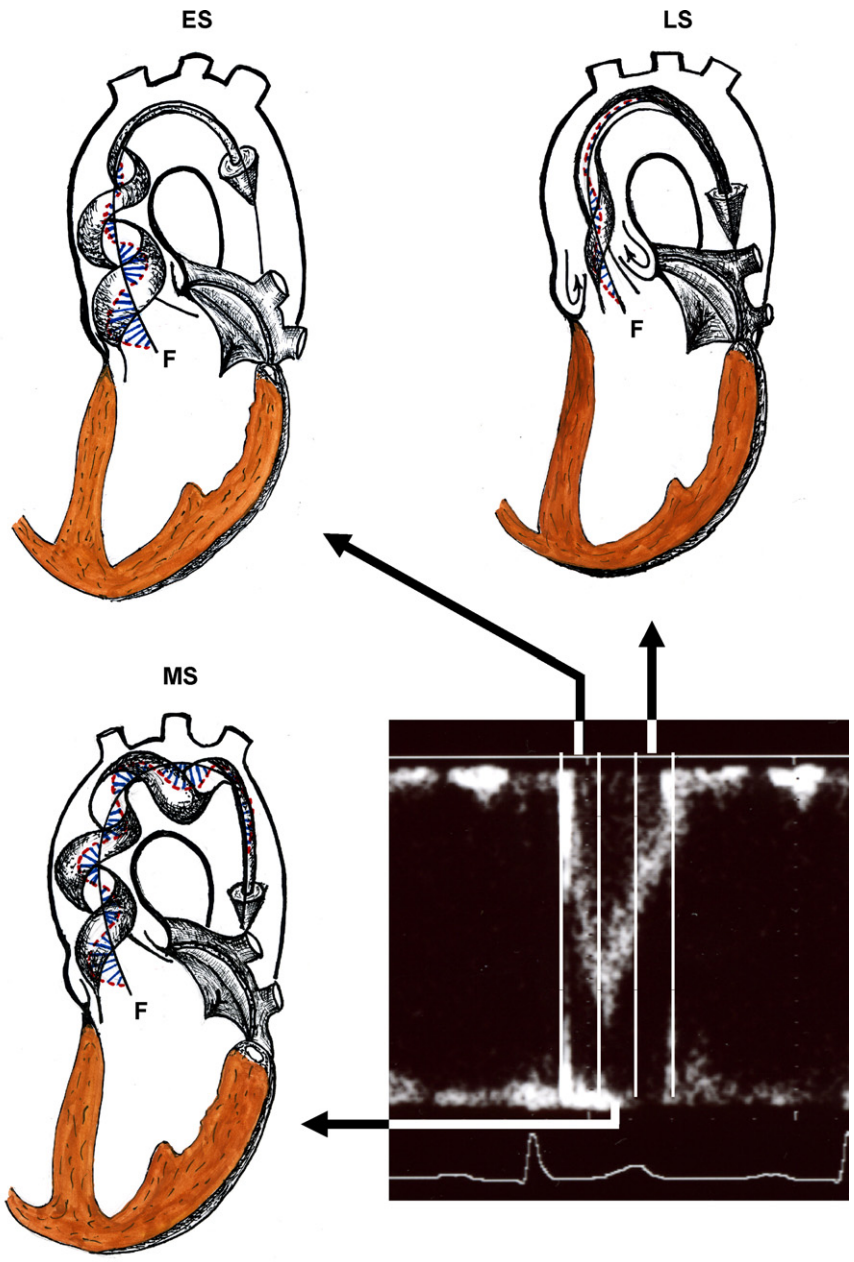

Figure 10 Schematic representation of the flow structure in the ascending aorta and aortic arch in ES, MS, and LS. Blue radial pattern indicates the changing acceleration of flow direction. ES, High accelerated flow due to the centrifugal force produced by the eddy just behind the anterior mitral leaflet passes the LV outflow antero-upward and the momentum extends the curvature of the aorta antero-upward and expands the basal part of the aorta. Thus the flow shifted antero-upward. However, both the expansion and extension are impeded by the rigidity of the surrounding tissues, and the ejected flow is imposed a large inertia resistance at the distal margin of the sinus of Valsalva. A part of the motion energy will be converted into the rotation energy. Thus, the ejected flow is reflected and turned over at the spherical concave inner surface of the antero-basal part of the aorta and the flow directs postero-downward, and the rotation begins. Then, the flow reflected again and turned over at the convex inner surface of the postero-inferior part of the arch. Thus the twisted spiral flow is produced. MS, The continuing rotation due to reflection and turn-over at the convex inner surface of postero-inferior part of the arch goes up to antero-upward and the second rotation occurs. Thereafter, the rotating flow turns over at the concave inner surface of the antero-upper part of the aorta. LS, The rotation continues and the twisted spiral flow progressed to the peripheral part. In this phase, the deceleration appears and the reversal flow occurs along the inner surface of the basal part of the aorta, and the vortex is produced in the sinus of Valsalva. ES, early systolic phase; MS, mid-systolic phase; LS, late systolic phase.

tion of the ejected flow was also demonstrated in the curved tube model.

Visualization of the flow in curved tube model using flat light method

The flow structure on the longitudinal cross-section examined using flat light method (Fig. 9) disclosed that bright lines from the reflector in the flow were longer along the under layer of the curved tube compared to those along the upper layer in the early stage of ejection. The flow velocity is faster in the under layer compared to those in the upper layer (Fig. 9, beginning stage).

During early and mid-stage, the length of the bright line was longer at the central area compared to that adjacent to the wall, where the line became shorter and decreased and finally converged toward the main flow axis line.

The main axis of the rotation flow in the curved tube was supposed to coincide with the center line of the tube. The flat-light method, which observed flow structure from the longitudinal cross-section, disclosed that the transit time of reflector passing through the flat light became long and the length of the bright line also became long at the central area, but the reverse was true at the area adjacent to the wall, confirming the occurrence of rotation flow during ejection.

Discussion

The results of the present study on the systolic blood flow structure in the ascending aorta and aortic arch are schematically shown in Fig. 10.

The accelerated blood flow in the cylindrical tube curved like the aorta inevitably ensures secondary flow due to viscosity, pressure gradient, centrifugal force, etc., and shows the high velocity component in the outside bend and low one in the inside bend and also the slowly rotating helical structure [2,6,7]. Peronneau et al. [5] demonstrated in dogs that the blood flow velocity distribution in the ascending aorta was higher at the inner (under) part of the arch and lower in the outer (upper) part. Kilner et al. [9] reported the right-handed helical flow in the ascending aorta in human subjects. Our data confirmed their results. In this respect, the data obtained by computer simulation were quite different from the present study observed in the human being.

Our results further revealed the upward displacement of the base of the aorta and distension of the arch as well as the diameter change. Therefore, the flow structure seemed to be complex including its rotation. However, the characteristics of such a flow structure have not been clarified yet.

Echo-dynamography enabled us to analyze 2D distribution of the velocity both in the longitudinal- and short-axis directions, vorticity, CAFD, and the development of the spiral twisted flow was definitely demonstrated. At the beginning of ejection, the high accelerated ejection flow forcefully displaced the basal part of the aorta antero-upward together with stretched curvature of the arch and expansion of the aorta. Thus the ejected flow shifted in the antero-upward direction and collided with and was reflected at the spherical concave inner surface of the antero-basal part of the aorta. A brisk clockwise rotation flow was observed in the basal part of the aorta including the sinus of Valsalva, and the spiral twisted flow appeared in the ascending aorta.

The occurrence of the spiral twisted flow will have the following three merits for: one, stabilizing the flow direction for passing through the curved pathway because the center of rotation always coincided with the center line of the aorta, two, maintaining the most effective flow volume by defeating the high inertia resistance because of the reversal correlation between the rotation rate and the maximum speed of the ejected flow, and three, dispersing the shear stress in the aortic wall which occurred by passing through the high accelerated flow. From the 2D distribution of the vorticity, it was considered that the rotating flow at the basal part of the aorta is produced by the momentum due to the high accelerated ejection flow in the early stage of ejection impeded by the rigidity of the surrounding aortic tissue. On the other hand, the distal margin of the sinus of Valsalva imposes a large inertia resistance from the peripheral aortic route. A part of the motion energy for ejection, which was equivalent to the velocity decrement and dynamic pressure increment (Fig. 2, ES, white arrow; Fig. 6, ES, black arrow), will be converted into rotation energy.

Though the tube experiment has no dilated part such as the sinus of Valsalva, the results were nearly the same as to the twisted spiral flow in the human beings. There may be a loose fixation of the entrance of the tube, but this experiment also clearly demonstrated the importance of the antero-upward displacement of the basal part together with shifting the flow direction antero-upward, the inertia resistance, and the curvature of the inner surface of the cylindrical curve of the tube to cause the spiral twisted flow.

Conclusion

Using echo-dynamography, the complicated systolic blood flow structure in the ascending aorta and arch was investigated.

During ejection, the twisted spiral flow was produced in the ascending aorta and arch, which started from the junction of the left ventricle and aorta and proceeded to the peripheral part. The cycle of the rotation inversely correlated with the maximum flow velocity. It is concluded that this twisted spiral flow is important to settle the direction of the accelerated blood flow under high pressure and is also helpful to disperse the shear stress in the aortic wall. Thus the blood was effectively ejected during the short period through the curved aortic pathway.

References

[1] Hwang NHC, Normann NA. Cardiovascular flow dynamics and measurement. Baltimore: University Park Press; 1977. pp. 1—216.

[2] Okino H, Sugawara M, Matsuo H. Cardiovascular dynamics and fundamental measurement. Tokyo: Kohdansha Co.; 1980. pp. 156—263.

[3] Nerem RM. Hot film measurement of arterial blood flow and observation of flow disturbances. In: Hwang NHC, Normann NA, editors. Cardiovascular flow dynamics and measurement. Baltimore: University Park Press; 1977. p. 191—215.

[4] Paulsen PK, Hasenkam JM. Three-dimensional visualization of velocity profile in the ascending aorta in dogs, measured with a hot-film anemometer. J Biomech 1983;16: 201—10.
[5] Peronneau PA, Hinglais JR, Xhaard M, Delouche P, Philippo J. The effects of curvature and stenosis on pulsatile flow in vivo and in vitro. In: Reneman RS, editor. Cardiovascular application of ultrasound. Amsterdam: North-Holland Publishing Co.; 1974. p. 203—15.
[6] Yearwood TL, Chandran KB. Physiological pulsatile flow experiments in a model of the human aortic arch. J Biomech 1984;15:683—704.
[7] Nakamura M, Wada S, Yamaguchi T. Computational analysis of blood flow in an integrated model of the left ventricle and the aorta. J Biomech Eng 2006;128:837—43.
[8] Segadal L, Matre K. Blood velocity distribution in the human ascending aorta. Circulation 1987;76:90—100.
[9] Kilner PJ, Yang GZ, Mohiaddin RH, Firmin DN, Longmore DB. Helical and retrograde secondary flow pattern in the aortic arch studied by three-directional magnetic resonance velocity mapping. Circulation 1993;88:2235—47.
[10] Tanaka M. Historical perspective of the development of echocardiography and medical ultrasound. In: Proc IEEE Ultrasonics Symp 2. 1998. p. 1517—24.
[11] Ohtsuki S, Tanaka M. The flow velocity distribution from the Doppler information on a plane in three dimensional flow. J Visual 2006;9:69—82.
[12] Tanaka M, Nitta S, Yamamoto A, Sato N, Takahashi K, Saijo Y, Ohtsuki S, Ohomote R, Ohba K, Ohno H. Development and application of non-invasive methods for the evaluation of cardiac function: measuring cardiac function. Asian Med J 1994;37:397—400.
[13] Ohtsuki S, Tanaka M. Flow function for streamline representative of the flow on a plane in three dimensional flow. J Visual Soc J 1998;18:136—40.
[14] Hino M. Introduction to fluid mechanics. Tokyo: Asakura Book Co.; 2002. pp. 41—9.
[15] Tanaka M, Sakamoto T, Sugawara S, Nakajima H, Katahira Y, Ohtsuki S, Kanai H. Blood flow structure and dynamics, and ejection mechanism in the left ventricle: analysis using echodynamography. J Cardiol 2008;52:86—101.
[16] Tanaka M, Nitta S, Yamamoto A, Takahashi K, Saijo Y, Ohtsuki S. Development and application of non-invasive method for the evaluation of cardiac function: visualization of pressure changes in heart chambers. Asian Med J 1994;37:341—4.
[17] Ohtsuki S, Tanaka M. Doppler pressure field deduced from the Doppler velocity field in an observation plane in a fluid. Ultrasound Med Biol 2003;29:1431—8.